The elongation of yeast prion fibers involves separable steps of association and conversion

Thomas Scheibel*†, Jesse Bloom‡, and Susan L. Lindquist*‡§¶

*Department of Molecular Genetics and Cell Biology and ‡Howard Hughes Medical Institute, University of Chicago, Chicago, IL 60637

Contributed by Susan L. Lindquist, December 31, 2003

A self-perpetuating change in the conformation of the translation termination factor Sup35p is the basis for the prion [*PSI*$^+$], a protein-based genetic element of *Saccharomyces cerevisiae*. In a process closely allied to *in vivo* conversion, the purified soluble, prion-determining region of Sup35p (NM) converts to amyloid fibers by means of nucleated conformational conversion. First, oligomeric species convert to nuclei, and these nuclei then promote polymerization of soluble protein into amyloid fibers. To elucidate the nature of the polymerization step, we created single-cysteine substitution mutants at different positions in NM to provide unique attachment sites for various probes. *In vivo*, the mutants behaved like wild-type protein in both the [*psi*$^-$] and [*PSI*$^+$] states. *In vitro*, they assembled with wild-type kinetics and formed fibers with the same morphologies. When labeled with fluorescent probes, two mutants, NM^{T158C} and NM^{E167C}, exhibited a change in fluorescence coincident with amyloid assembly. These mutants provided a sensitive measure for the kinetics of fiber elongation, and the lag phase in conversion. The cysteine in the mutant NM^{K184C} remained exposed after assembly. When labeled with biotin and bound to streptavidin beads, it was used to capture radiolabeled soluble NM in the process of conversion. This process established the existence of a detergent-susceptible intermediate in fiber elongation. Thus, the second stage of nucleated conformational conversion, fiber elongation, itself contains at least two steps: the association of soluble protein with preformed fibers to form an assembly intermediate, followed by conformational conversion into amyloid.

Yeast prions are protein-based elements of inheritance. They propagate by a mechanism that resembles the self-perpetuating alteration of protein conformation found in prion-based encephalopathies, noninfectious neurodegenerative diseases, and systemic amyloidoses. However, they do not cause disease. Rather, they create epigenetically inherited phenotypes (1). One yeast prion protein, Sup35p, is a translation termination factor. Normally, it is soluble and fully functional. However, when it converts to the prion state, there is a change in the efficiency of translation termination. This phenotypic change is heritable because protein with the altered conformation is passed from the cytoplasm of mother cells to their daughters, perpetuating the cycle of conformational change (2–5).

The *in vivo* conversion of Sup35 protein from the nonprion [*psi*$^-$] state to the prion [*PSI*$^+$] state is closely modeled *in vitro* by the self-seeded conformational conversion of the soluble Sup35p into amyloid fibers. The prion-determining region of Sup35 (NM) is the most tractable to work with *in vitro*. It is referred to as NM, because it consists of the N-terminal asparagine and glutamine-rich region and the middle glutamate and lysine-rich region. Strikingly, purified, soluble NM is induced to change into amyloid fibers when seeded by lysates of [*PSI*$^+$] but not [*psi*$^-$] cells (2, 6, 7). Moreover, mutations that enhance or inhibit [*PSI*$^+$] propagation *in vivo* also enhance or inhibit NM conversion into amyloid *in vitro* (8, 9).

Understanding the molecular mechanism of protein-based inheritance is itself of great interest in genetics (10, 11). In addition, the ability to combine yeast genetic methods with biochemical analyses makes NM an excellent model for elucidating the general process of amyloid self-assembly, which is of fundamental importance in human biology and medicine (12). Moreover, the self-assembly properties of NM, together with the stability of the fibers it forms and the various methods available for their functional modification, provide promise for the production of nanometer-scale devices in material sciences (13). Here, we develop tools for assaying NM assembly and apply them to investigating a particular stage in the polymerization process.

Amyloid polymerization generally starts with the formation of a nucleus that contains protein with a different conformation than that of soluble protein. The nucleus promotes the conformational conversion of the remaining soluble protein into amyloid fibers (14–22). The polymerization of NM is also a two-stage process (2–4). When denatured NM is initially diluted into physiological buffers it has the features of an intrinsically unstructured (random coil-rich) protein (23). After a lag phase, nuclei form and initiate the rapid conversion of soluble NM into β-sheet-rich amyloid.

We have proposed that nucleation occurs through a previously unrecognized process: an equilibrium is established between NM monomers and relatively unstructured detergent-soluble oligomers and it is the concerted conformational conversion of proteins within these oligomers that produces nuclei to seed polymerization (3). This model is distinct from those for other nucleated polymerization reactions, such as that of α-synuclein, in which protein monomers that have already acquired the conformation that is characteristic of the fiber state come together in sufficient numbers to form a stable nucleus, which seeds through a process akin to crystallization (24). Different processes may govern the assembly of different amyloids (25), but recent data (3) suggest that at least some of the amyloids implicated in neurodegenerative disease may assemble from a conformationally molten oligomeric intermediate, similar to that which we had proposed for NM. We have called this process nucleated conformational conversion (NCC).

In this paper, we seek to understand how nuclei mediate the conversion of soluble NM to the amyloid form in the elongation phase of fiber formation. Conversion of NM has been monitored previously by changes in far-UV CD, SDS solubility, protease sensitivity, morphology by atomic force microscopy, and Congo red and Thioflavin T binding (2–4). Here, we took advantage of the fact that NM does not contain any cysteine residues to create more sensitive tools for polymerization studies. We made use of a previously established series of individual cysteine substitution mutations at several locations in NM (26). All were tested and

BIOCHEMISTRY

Abbreviations: NM, prion-determining region of Sup35; NM^{cys}, cysteine-substituted NM; NM^{wt}, wild-type NM; GdmCl, guanidinium chloride; NCC, nucleated conformational conversion; acrylodan, 6-acryloyl-2-dimethylaminonaphthalene; IANBD amide, *N*,*N*′-dimethyl-*N*-(iodoacetyl)-*N*′-(7-nitrobenz-2-oxa-1,3-diazol-4-yl)ethylenediamine.

†Present address: Institut für Organische Chemie und Biochemie, Technische Universität München, D-85747 Garching, Germany.

§Present address: Whitehead Institute for Biomedical Research, Cambridge, MA 02142.

¶To whom correspondence should be addressed at: Whitehead Institute for Biomedical Research, Nine Cambridge Center, Cambridge, MA 02142-1479. E-mail: lindquist_admin@wi.mit.edu.

established to behave like wild-type protein *in vivo*. The nature of the seeded assembly process was then investigated by attaching fluorescent and radioactive probes to the cysteines. This analysis established that elongation itself is a two-step process involving the capture of an intermediate, followed by its conformational conversion.

Materials and Methods

Sedimentation of Assembled Intermediates. Assembly reactions of NM^{T158C}-6-acryloyl-2-dimethylaminonaphthalene (acrylodan) were started by addition of wild-type NM (NM^{wt}) seed (4% wt/wt) at distinct time points to produce a time course. All samples were sedimented simultaneously at 130,000 × *g* for 2 min at 25°C in an Optima TL ultracentrifuge (Beckman) by using a TLA100.2 rotor. The supernatant was removed for fluorescence analysis to quantify the remaining soluble protein (*S*).

Radioactivity Assay to Detect Assembly Intermediates. Seeds were prepared from NM^{K184C} by sonication of fibers, creating 100- to 500-nm-long short fibers with a high seeding efficiency. Such seeds were biotinylated as described (26). NM^{T158C} was labeled with iodo[1-^{14}C]acetamide (Amersham Pharmacia). Reactions were started by addition of NM^{K184C} seed (50% wt/wt), which has an indistinguishable seeding efficiency in comparison with NM^{wt} (26), and aliquots of the reaction were incubated for two min with Streptavidin-coated M-280 Dynabeads (Dynal) at distinct time points after starting the reaction. After fixing the Dynabeads with a Dynal MPC magnet, the supernatant was removed and the beads were washed, which took ≈30 s. Protein that was bound to the immobilized fibers, but still not converted (assembly intermediate; *SA*), was resolubilized by incubating the samples for 1min with 2% SDS. The SDS elution fraction was quantified for ^{14}C-radioactivity, and the remaining immobilized fibers were monitored for efficient incorporation of ^{14}C-labeled NM^{T158C} by scintillation counting.

Details of the materials and methods for bacterial strains, cell culture, mutagenesis, protein purification, light scattering, fluorescent labeling of cysteine-substituted NM (NM^{cys}), curve fits, electron microscopy, and yeast strains can be found in *Supporting Materials and Methods*, which is published as supporting information on the PNAS web site.

Results and Discussion

Mutation-Based Analysis of Higher-Order Structural Changes. To provide new tools for the *in vitro* analysis of NM assembly we engineered unique sites for the covalent attachment of a variety of biophysical probes. Because wild type NM (NM^{wt}) does not contain cysteine residues, we introduced NM^{cys} distributed throughout, with each mutation carrying just one substitution to provide a unique location for attachments (NM^{S2C}, NM^{Y35C}, NM^{Q38C}, NM^{Q40C}, NM^{G43C}, NM^{G68C}, NM^{M124C} NM^{L144C}, NM^{T158C}, NM^{E167C}, NM^{K184C}, NM^{E203C}, NM^{S234C}, and NM^{L238C}; ref. 26). Three of the mutants, NM^{Y35C}, NM^{Q40C}, and NM^{M124C}, were not expressed recombinantly in *Escherichia coli* at a level sufficient for *in vitro* analysis and were not studied further.

All other mutants were tested *in vivo* for their ability to function like wild-type Sup35p, by replacing the NM region of the genomic wild-type copy of *SUP35* with each of the *Sup35^{cys}* variants by site-directed gene conversion in the yeast strain *74-D694*. Replacements were performed both in [*psi*$^-$] and [*PSI*$^+$] cells (26). All of Sup35^{cys} proteins were stably expressed at levels indistinguishable from that of Sup35p^{wt} (data not shown). All stably maintained the [*psi*$^-$] phenotype in [*psi*$^-$] cells and the [*PSI*$^+$] phenotype in [*PSI*$^+$] cells. Further, when [*psi*$^-$] and [*PSI*$^+$] cells were mated *inter se*, as expected with cytoplasmic inheritance, the [*PSI*$^+$] state was dominant and segregated 4:0 in progeny. In the [*PSI*$^+$] state, each of the mutants efficiently converted [*psi*$^-$] cells to [*PSI*$^+$] by cytoduction, the exchange of cytoplasm without nuclear transfer (data not shown). Finally, each was cured of the [*PSI*$^+$] state by growth on plates containing 5 mM GdmCl. Thus, all of the mutants behaved like wild-type protein with respect to the full spectrum of epigenetic characteristics of the [*psi*$^-$] and [*PSI*$^+$] states.

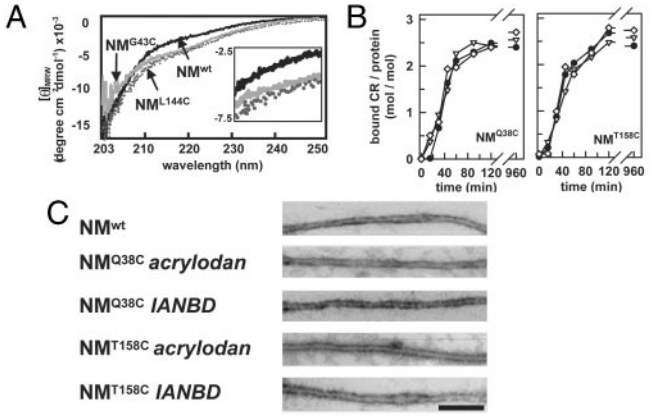

Fig. 1. Structural comparison of NM^{wt} with NM^{cys} mutants. (*A*) Structural comparison of NM^{wt} (solid black band), NM^{G43C} (solid gray band), NM^{L144C} (shaded gray band) by far-UV CD spectra. (*Inset*) The spectra between 210 and 220 nm with a higher magnification. (*B*) Fiber assembly of fluorescently labeled NM^{cys} mutants. NM^{Q38C} and NM^{T158C} (5 μM each) are shown as representative examples, as detected by Congo red binding: unlabeled (●), acrylodan labeled (▽), and IANBD amide-labeled (◇). (*C*) Electron micrographs show individual NM^{cys} fibers with covalently attached acrylodan or IANDB amide as indicated. (Bar, 100 nm.)

Next, each of the purified mutant proteins was analyzed *in vitro* in NM assembly reactions. All assembled into β-sheet-rich fibers in seeded and unseeded reactions, and seven mutants had slightly different assembly kinetics, produced shorter fibers, or had molar ellipticity values at 222 nm, which were somewhat different from wild-type (Fig. 1*A* and data not shown). Only the mutants NM^{S2C}, NM^{Q38C}, NM^{T158C}, and NM^{E167C} were completely indistinguishable from NM^{wt} by every criteria examined.

Fluorescent Labeling of NM^{cys}. We labeled these four mutant proteins with acrylodan and, separately, with *N*,*N*′-dimethyl-*N*-(iodoacetyl)-*N*′-(7-nitrobenz-2-oxa-1,3-diazol-4-yl)ethylenediamine (IANBD amide). Both fluorescent labels are commonly used to detect protein conformational changes and assembly because their fluorescent properties vary depending on solvent accessibility (27–30). The labeling efficiency ranged from 0.40 to 0.78 M label/M protein, as determined by UV/Vis absorption spectrophotometry, depending on the mutant and label used. Nonspecific labeling, assessed with NM^{wt}, was <0.05 M/M (data not shown).

To determine whether the labels themselves affected fiber assembly, mixed-assembly reactions were performed with equal quantities of labeled and unlabeled protein of each mutant. The ratio of labeled protein to unlabeled protein that remained in the soluble phase was constant throughout the assembly time course (data not shown), and the final level of assembly was the same (Fig. 1*B* and data not shown). The fibers formed with each of the labeled NM^{cys} mutants were indistinguishable from unlabeled NM^{cys} fibers in terms of their diameter (11.5 ± 1.5 nm) and concentration (Fig. 1*C* and data not shown). Thus, covalent attachment of acrylodan/IANBD amide did not influence the assembly of these mutants.

Fluorescence Assay for Conformational Conversion. Next, we asked which residues were located in positions that would provide a change in fluorescent signal on assembly in conformational

conversion reactions (during seeded fiber elongation). For all four NM^{cys} mutants tested, acrylodan showed a blue shift in fluorescence emission maximum (λ_{max}), indicating that the environment of each cysteine substitution changed. To determine whether these changes were based on the conformational transitions that are associated with the transition from soluble protein into fibers, fluorescent changes were analyzed for 12 h in undisturbed, nonseeded reactions. Such reactions depend on spontaneous nucleation, and no NM fibers are detected in this time frame (4). This experiment revealed that acrylodan fluorescence emission showed a gradual change of λ_{max} during the preassembly stage for NM^{S2C} and NM^{Q38C} (data not shown). The N region of NM has by many criteria been established as the region responsible for nucleation. Thus, these changes most likely reflect early conformational transitions involved in the first stage of NCC, and warrants further study.

Acrylodan fluorescence emission of NM^{T158C} and NM^{E167C}, both located in the M region, revealed no significant change after 12 h in nonseeded samples (Fig. 2*A* and data not shown). However, coincident with seeded fiber assembly, solutions of NM^{T158C}- and NM^{E167C}-acrylodan showed increased fluorescence intensities, accompanied by a blue shift of λ_{max} (NM^{T158C}: 521 to 486 nm, Fig. 2*A*; NM^{E167C}: 528 to 502 nm). Thus, acrylodan labels at cysteine 158 and 167 are sensitive to the conformational differences between soluble and fibrous NM.

Seeded Fiber Elongation Occurs in Two Steps. In the second stage of NCC, soluble protein is converted into amyloid fibers by the nuclei. Nucleation of fiber assembly can be bypassed by the addition of preformed fibers to soluble protein (3, 4). Both NM^{T158C}- and NM^{E167C}-acrylodan (2 μM each) showed a rate of fiber assembly of $v^{fluor} = 8 \pm 0.4 \times 10^{-4}$ μmol·s^{-1} at 25°C (Fig. 2*B* and data not shown) in the presence of seed (4% wt/wt). At this seed concentration soluble NM is present in excess over the seeding fiber ends by ≈50,000-fold (3). This fiber assembly rate was similar to that measured for NM^{wt} by far-UV CD (3×10^{-4} μmol·s^{-1}; refs. 3 and 4) and light scattering ($5 \pm 0.3 \times 10^{-4}$ μmol·s^{-1}) at identical experimental conditions.

To determine the kinetic parameters of fiber assembly, it was essential to ensure that both the substrate and the seed concentrations were not limiting in the reactions. Therefore, we determined fiber assembly rates with constant seed concentrations (4% wt/wt calculated for a 5 μM protein concentration) and varying soluble protein concentrations. Decreasing the soluble NM concentration 100-fold only decreased fiber assembly rates by a factor of two (Fig. 2*B*). Hence, we are confident that soluble protein is in excess with 4% wt/wt of seed and 5 μM soluble NM.

The kinetics of seeded fiber elongation reproducibly showed a lag-phase of 80 ± 10 s at 25°C, then exhibited linear kinetics (Fig. 2*C*). The delay in fiber assembly suggested that an assembly intermediate is formed. To confirm the existence of an intermediate, we took advantage of the fact that nonfibrous NM is soluble in SDS, whereas fibrous NM shows SDS resistance (3). Based on this determination, we developed an assay to detect intermediate complexes; i.e., soluble NM that is associated with seed but not converted into the fiber state. Seeds were prepared from NM^{K184C}, a cysteine-substitution mutant with surface-accessible sulfhydryl groups that allows labeling after fiber formation and that has a seeding efficiency indistinguishable to that of NM^{wt} (26). These NM^{K184C} seeds were biotinylated as described (26). Further, NM^{T158C} was labeled with iodo[1-^{14}C]acetamide. Reactions were started by addition of biotinylated NM^{K184C} seed (50% wt/wt) to soluble NM^{T158C}-iodo[1-^{14}C]acetamide. At distinct time points aliquots of the reaction were incubated with Streptavidin-coated Dynabeads. A high ratio of seed to soluble protein was used to ensure that the fiber ends (i.e., the seeds) were saturated with soluble NM, to allow the best opportunity of observing short-lived intermediate complexes. The beads were removed at different time points by using a magnet and washed with SDS to detect nonconverted intermediates. Both the SDS-soluble protein and the SDS-resistant fibers, which were attached to the beads, were analyzed by scintillation counting (Fig. 2*D*). At early time points, a substantial fraction (≈50%) of the NM assembled with bead-bound seeds was soluble in SDS, at later time points the fraction of SDS-soluble material diminished. In a control experiment, in which the NM^{K184C} seeds were not biotinylated, no radioactivity could be detected attached to the beads. The ability to capture material bound to the seed that had not completely converted, established the formation of a detergent susceptible complex. However, this method did not have sufficient resolving power to analyze kinetic parameters of the assembly process.

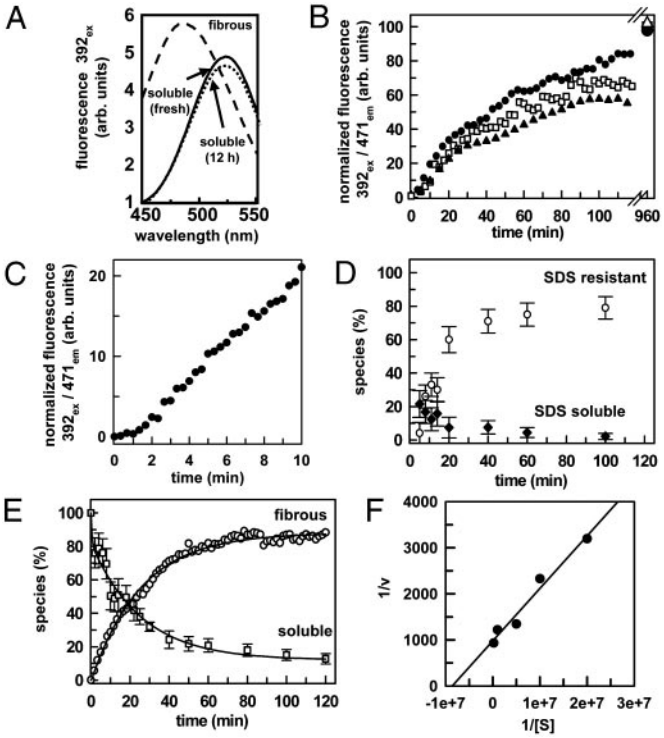

Fig. 2. Conformational conversion can be determined by acrylodan fluorescence changes, with excitation at its absorption maximum of 392 nm and the maximal fluorescence emission difference at 471 nm. (*A*) Fluorescence emission wavelength scans of NM^{T158C}-acrylodan (2 μM) at 25°C: freshly diluted protein (solid line), fluorescence after 12 h (dotted line) (no fibers were detected by Congo red-binding or electron microscopy), and fluorescence after 12 h in seeded reactions with detectable amyloid fibers (dashed line). (*B*) Concentration dependence of fiber elongation of NM^{T158C}-acrylodan with a constant seed concentration (4% wt/wt) calculated for a 5-μM solution at 25°C. The fluorescence intensities were normalized for direct comparison at 0.05 (▲), 0.5 (□), and 5 (●) μM. (*C*) Lag time of fiber elongation of NM^{T158C}-acrylodan (2 μM) with a constant seed concentration (4% wt/wt), calculated for a 5-μM solution. (*D*) Species distribution during seeded fiber elongation of NM^{T158C}-iodo[1-^{14}C]acetamide (2 μM) starting with soluble (100%) and unconverted (0%) NM^{T158C}- iodo[1-^{14}C]acetamide. Fiber elongation is initiated by addition of biotinylated NM^{K184C} seed (50% wt/wt): converted fibrous protein (SDS-resistant) (○) and assembly intermediate (SDS soluble) (♦). (*E*) Species distribution during seeded fiber elongation of NM^{T158C}-acrylodan (2 μM), as determined independently in a sedimentation and a fluorescent wavelength shift assay, starting with soluble (100%) and unconverted (0%) NM^{T158C}-acrylodan. Fiber elongation is initiated by addition of seed: converted protein (fibrous) (○) and soluble protein (□). All lines represent curve fits by using SCIENTIST (MicroMath, St. Louis). (*F*) Lineweaver–Burk plot to determine kinetic parameters of NCC. The double reciprocal plot yields a straight line, in which the *x* intercept gives $-1/K_m$ and the *y* intercept = $1/V_{max}$.

To establish kinetic parameters, it was necessary to precisely discriminate between soluble and seed-bound NM. Therefore, we developed a sedimentation assay to detect the disappearance of soluble NM^{T158C}-acrylodan during fiber assembly. The total acrylodan concentration was plotted against its concentration in the supernatant, and each measurement was repeated six times to estimate the variation (Fig. 2*E*). In combination with the wavelength shift assay (above), this assay provided data to kinetically analyze fiber assembly and develop a model for nucleated fiber elongation. These reactions have two reactants: the seed and the soluble NM, with the soluble NM as the substrate being in excess of the seed, and a catalyst that is not used up as the reaction progresses (the catalyst is the fiber ends, to which the soluble NM bind, but the same number of ends are present as the fiber elongates). These components and that these reactions reach steady state kinetics suggest that they can be analyzed with the Michaelis–Menten equation used to describe enzyme kinetics:

$$S + A \underset{k_{-1}}{\overset{k_1}{\longleftrightarrow}} SA \xrightarrow{k_{conf}} AA$$

where S is soluble NM, A is assembled protein (seed), SA is bound but not converted intermediate (akin to an enzyme:substrate complex), and AA is converted fiber, which again can act as seed. Importantly, we were unable to discriminate whether seed associates with monomers or oligomers or both. The observed rate of conformational conversion is determined experimentally by k_1 and k_{-1}, the rate constants for binding and dissociation, and k_{conf}, the first-order conformational conversion rate. Because the dissociation rate of converted protein from the amyloid fibers is too slow to be detected in our experimental set-up, the back reaction

$$AA \rightarrow SA$$

is quasi-irreversible and is ignored in our model. We analyzed our experimental data by using a Lineweaver–Burk plot (Fig. 2*F*), which yielded a straight line and a protein concentration of $K_m = 0.12 \pm 0.01$ μM, at which the rate of reaction is half of the maximum rate. We also calculated a maximal rate of conformational conversion $V_{max} = 10 \pm 0.3 \times 10^{-4}$ μmol·s^{-1}, the rate constant of conformational conversion of $k_{conf} = 5 \pm 0.1 \times 10^{-3}$ s^{-1}, and a conformational conversion efficiency of $k_{conf}/K_m = 42{,}000$ M^{-1}·s^{-1}, which is equivalent to an enzyme's specificity constant.

Influences of Temperature on Seeded Fiber Elongation. We investigated the effect of increased temperature on seeded fiber elongation with NM^{T158C}-acrylodan in the presence of 4% wt/wt of seed, because previous studies detected an inhibitory effect of elevated temperature (4). In accordance to the previous study, we found a low-temperature optimum for the rate of fiber assembly as seen in the logarithm of NCC velocities plotted against the reciprocal temperature (Arrhenius plot; Fig. 3*A*, 4% seed). The sticking probability of soluble protein, which is reflected by k_{conf}/k_{-1}, characterizes the rate at which soluble NM associates with seed relative to dissociation; i.e., the sticking probability is high if $k_{-1} < k_{conf}$. In our experiments, the abnormal temperature dependence with decreasing ratios of k_{conf}/k_{-1} at elevated temperature indicates a significant rate enhancement for the dissociation of the seed-NM (SA) complex in comparison to its conversion into an assembled fiber (AA). At low temperature $k_{-1} \ll k_{conf}$ and k_{conf}/K_m becomes equal to k_1. Because the dissociation of nonconverted, but seed-bound NM, has a high activation energy, k_{-1} becomes predominant at high temperature.

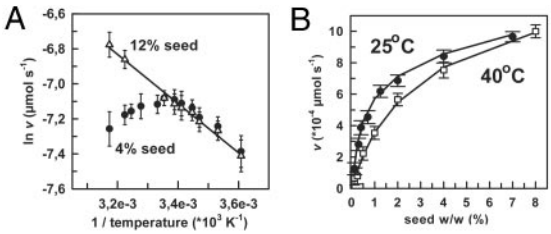

Fig. 3. The first rate-determining step of fiber elongation is temperature-dependent. (*A*) The logarithm of fiber elongation velocities with a constant soluble NM concentration of 2 μM by using 4% wt/wt of seed (●) and 12% wt/wt of seed (△) are plotted against the reciprocal temperature (Arrhenius plot). (*B*) Fiber elongation velocities starting with soluble NM^{T158C}-acrylodan (1 μM) are plotted against the percentage of seed added (wt/wt) at 25°C (●) and 40°C (□).

To test this hypothesis experimentally, we measured the velocities of fiber elongation at 25°C and 40°C with a constant soluble NM^{T158C}-acrylodan concentration (2 μM) and increasing seed concentrations. We confirmed that increasing seed concentrations led to increasing fiber elongation velocities at both temperatures yielding maximal elongation rates at >10% wt/wt of seed (Fig. 3*B*). Therefore, we plotted fiber elongation velocities at 12% wt/wt of seed, which should be a non-rate-limiting seed concentration for fiber elongation, against the reciprocal temperature. The plot revealed a temperature dependence of fiber elongation that is consistent with the collision theory of Arrhenius (Fig. 3*A*, 12% seed). The Arrhenius plot gives a straight line and its slope is equivalent to the activation energy E_a divided by the gas constant $R = 8.3145$ J K^{-1}·mol^{-1}. By using this equation, the activation energy for fiber elongation was calculated to be $E_a = 11.7 \pm 0.2$ kJ mol^{-1}.

Acquisition of Secondary and Tertiary Structure of Soluble NM. To elucidate the influence of the conformation of soluble NM on the association with seed, we investigated the rate at which secondary, tertiary, and quaternary structures were acquired in soluble material. When NM is first diluted out of denaturants such as urea or guanidinium chloride (GdmCl), it adopts the characteristics of a molecule that is rich in random coil (typical for intrinsically unstructured proteins; ref. 23), indistinguishable from NM purified under nondenaturing conditions (4). To analyze whether the rate of this process influences seeded fiber assembly, we used 6 M GdmCl to form a homogenous and monomeric population of denatured NM (Fig. 4*D*). After dilution into 5 mM sodium phosphate, pH 7.4, 150 mM NaCl, we monitored the time course of far-UV CD changes at 222 nm (refs. 4 and 26 and Fig. 4*A*). The acquisition of secondary structure reached half-maximal amplitude after 24 ± 2 s with a rate constant of $k_{gain}^{farUV} = 2.1 \pm 0.2 \times 10^{-2}$ s^{-1}. Thus, the formation of secondary structure is not rate determining for seeded fiber elongation.

The kinetics of acquisition of NM tertiary structure was investigated by using the four fluorescently labeled NM^{cys} mutants. Changes in tertiary structure of NM on dilution into buffer from 6 M GdmCl were investigated with two different techniques: IANDB amide-labeled protein was detected by fluorescence emission, and acrylodan-labeled protein was detected with near-UV CD. The fluorescence emission of IANBD amide revealed solvent exposure in all four mutants in 6 M GdmCl, as expected. A stable IANDB amide emission signal was reached after dilution into buffer indicative of a higher ordered environment. The time course had a half-maximal amplitude at 31 ± 4 s and a rate constant of $k_{gain}^{fluor} = 1.6 \pm 0.2 \times 10^{-2}$ s^{-1} (Fig. 4*B* and data not shown). Similarly, near-UV CD time courses with acrylodan-labeled NM (all four mutants led to the same results) showed a half-maximal

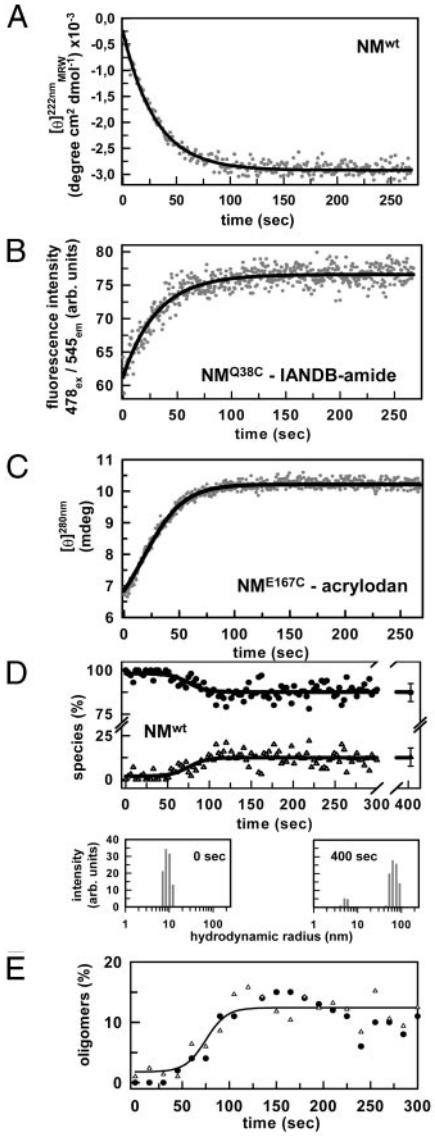

Fig. 4. Structural gain of NM after dilution out of GdmCl. (*A*) Secondary structure gain of NM^{wt} (5 μM) after dilution out of 6 M GdmCl (final concentration: 50 mM) into 5 mM potassium phosphate (pH 7.4), 150 mM NaCl measured by far-UV CD (222 nm). The kinetics are independent of protein concentration between 0.5 and 65 μM (data not shown) and follow a single exponential with the rate constant $k_{gain}^{far} = 2.1 \pm 0.2 \times 10^{-2}\ s^{-1}$. (*B*) NM^{Q38C}-IANBD amide (5 μM) fluorescence indicates a rate constant for tertiary structure gain of $k_{gain}^{fluor} = 1.6 \pm 0.2 \times 10^{-2}\ s^{-1}$. (*C*) Near-UV CD at 280 nm, which best describes the tertiary structure changes of NM^{E167C}-acrylodan (5 μM), indicates a rate constant for tertiary structure gain of $k_{gain}^{nearUV} = 1.5 \pm 0.1 \times 10^{-2}\ s^{-1}$. (*D*) Time course of NM^{wt} (5 μM) oligomerization by quasi-elastic light scattering: monomeric NM^{wt} (●) and oligomeric NM^{wt} (△). In a steady state, NM monomers represent 87 ± 5% (mass-normalized; *Upper*), with hydrodynamic radii of 4 ± 1 nm (monomer) and 50–130 nm (oligomers) (intensity-normalized; *Lower*). In 6 M GdmCl, NM^{wt} shows a hydrodynamic radius of 9 ± 2 nm. The data are corrected for the change in viscosity with GdmCl concentration. (*E*) Concentration independence of NM^{wt} oligomerization by dynamic light scattering. Only oligomeric species are shown at 1 (●) and 40 μM (△). The oligomerization is temperature independent (data not shown). The solid lines represent single exponential fits.

amplitude after 33 ± 2 s and a rate constant of $k_{gain}^{nearUV} = 1.5 \pm 0.1 \times 10^{-2}\ s^{-1}$ (Fig. 4*C* and data not shown). Both independent measurements revealed that formation of some tertiary structure is also not rate limiting for seeded fiber assembly under the experimental conditions chosen.

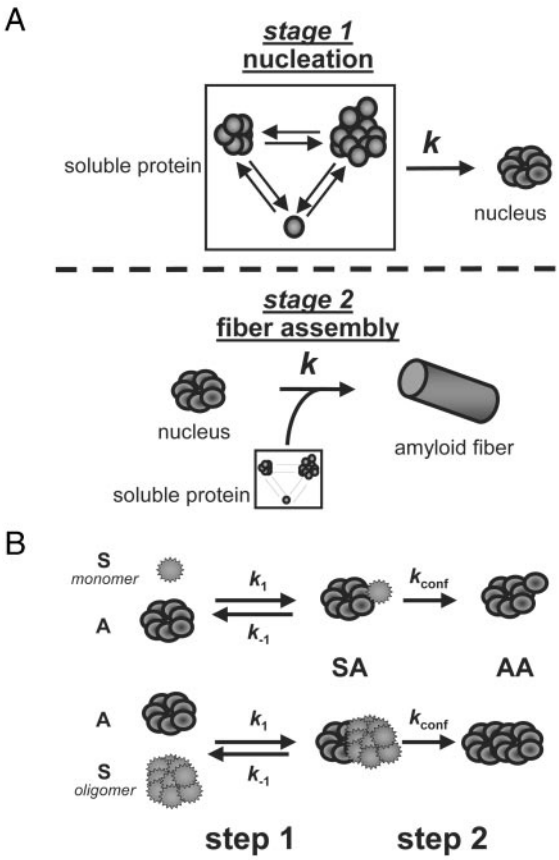

Fig. 5. (*A*) NCC of NM is a two-stage process. The soluble state of NM is a steady state between monomers and oligomers. These oligomers are not well defined and do not promote NCC, but they are converted into a nucleus over time in stage 1. This nucleus initiates conformational conversion of additional soluble protein into amyloid fibers in stage 2. (*B*) Seeded fiber elongation imitates the second stage of NCC and requires two steps. The first step is the protein–protein interaction between soluble NM (S) and nuclei/seed (A) with k_1 and k_{-1} representing the rate constants for binding and dissociation. The second step is conformational conversion of deposited NM (SA) into the final amyloid structure (AA) with the first-order conformational conversion rate k_{conf}.

Quaternary Structure Analysis. Dilution of NM^{wt} out of denaturant led to the formation of a mixed population of monomers (87 ± 5%) and heterogeneous oligomers, with varying molecular masses from tetramers to 30-mers (Fig. 4*D*). Oligomerization was preceded by a lag phase of ≈60 s after dilution out of denaturant, which suggests that some acquisition of secondary and tertiary structure is required before oligomerization. Populations of monomers and oligomers were established after a half-time of 75 ± 5 s and remained constant for 3 h (Fig. 4*D Upper*). Because this steady state was achieved far before spontaneous nucleation (and well before seed was added), NM oligomerization is not likely to be rate determining for seeded fiber assembly in our experiments.

Our data suggested the following mechanism for initial structural changes of soluble NM, starting from the denatured state:

$$xM_u \xrightarrow{k_{gain}} xM \rightleftharpoons O_x$$

where M_u is the unfolded monomer, M is the random-coil monomer with some structure, and O_x are the oligomers. The rate constant for structural gain of monomeric NM from the

BIOCHEMISTRY

denatured state was $k_{gain} = 1.5 \pm 0.2 \times 10^{-2}$ s^{-1}. Remarkably, the rate of oligomerization and establishment of a steady-state distribution of monomers and oligomers showed little dependence on the concentration of NM between 0.7 and 46 μM (Fig. 4*E*). This observation agrees with a previous study (3) where NM fiber assembly proceeds by means of the conversion of oligomers to nuclei with little concentration dependence. Nuclei form by conformational rearrangements of NM within the context of oligomeric intermediates and not by assembly of structurally converted monomers (3).

Implications. Self-perpetuating conformational conversion of NM is responsible for epigenetic inheritance of an altered conformational state in yeast. Previous work proposed that conformational conversion follows a mechanism of NCC (ref. 3 and Fig. 5), which is similar to that for conformational conversion of Alzheimer's A-β and islet amyloid polypeptide, suggesting that it may be widely applicable for describing amyloid fibrillogenesis, especially for intrinsically unstructured proteins (17, 31, 32). Because high-resolution techniques to analyze mechanistic details of NCC are unavailable, we used a generally applicable, sensitive method that measures changes in the intrinsic fluorescence of residues whose environments change during conformational transitions.

Oligomerization of NM is necessary to form nuclei. Here, we determined that oligomerization of soluble NM is not strongly dependent on the concentration on NM. Further, we found that the rate of oligomerization cannot be rate limiting in the first stage of NCC. It is, rather, a structural rearrangement of oligomers: most likely some oligomers convert to a conformational state competent for nucleation during prolonged incubation (Fig. 5). However, to investigate this first stage and to resolve the mechanistic details of NCC, it is crucial to first define the steps of the second stage.

The second stage of NCC can be imitated when a sufficient amount of preformed fibers (seed) is added to soluble NM. We identified two rate-determining steps of the second stage of NCC by using seeded reactions: (*i*) binding of soluble protein to the seed and (*ii*) conformational conversion initiated by the seed (Fig. 5). We have not determined the soluble protein fraction (monomeric, oligomeric, or both) that interacts with seed. At 25°C, soluble NM (*S*) dissociates more slowly from the complex with seed (*SA*) than it is converted. However, dissociation of nonconverted, but seed-bound NM, becomes predominant at high temperature. The final step of conformational conversion is quasi-irreversible under steady growth conditions, which are obtained by continuously adding new protein at the seeding ends, leading to the formation of amyloid fibers.

It has been shown recently for another amyloid, transthyretin, that amyloidoses inhibitors prevent amyloid formation by stabilizing the native state (33). Our results highlight a possibility that inhibition of amyloid assembly with chemicals that influence the association/dissociation properties of soluble protein with preexisting amyloid fibers might also be successful. Furthermore, our results contribute to understanding how to control amyloid formation kinetically, which will aid in the development of materials, and in the elucidation of protein-based mechanisms of inheritance and processes leading to protein-folding diseases.

We thank Anthony Kowal and Dan Vatner for experimental assistance, members of the Lindquist Laboratory, and Stefan Walter for critical comments on the manuscript. This work was supported by National Institutes of Health Grant GM57840, the W.M. Keck Foundation, the Howard Hughes Medical Institute, and Deutsche Forschungsgemeinschaft Postdoctoral Fellowship SCHE 603/1-1 (to T.S.).

1. Koo, E. H., Lansbury, P. T. & Kelly, J. W. (1999) *Proc. Natl. Acad. Sci. USA* **96,** 9989–9990.
2. Glover, J. R., Kowal, A. S., Schirmer, E. C., Patino, M. M., Liu, J. J. & Lindquist, S. (1997) *Cell* **89,** 811–819.
3. Serio, T. R., Cashikar, A. G., Kowal, A. S., Sawicki, G. J., Moslehi, J. J., Serpell, L., Arnsdorf, M. F. & Lindquist, S. L. (2000) *Science* **289,** 1317–1321.
4. Scheibel, T. & Lindquist, S. (2001) *Nat. Struct. Biol.* **8,** 958–962.
5. DePace, A. H. & Weissman, J. S. (2002) *Nat. Struct. Biol.* **9,** 389–396.
6. Paushkin, S. V., Kushnirov V. V., Smirnov V. N. & Ter-Avanesyan, M. D. (1997) *Science* **277,** 381–383.
7. Uptain, S. M., Sawicki, G. J., Caughey, B. & Lindquist, S. (2001) *EMBO J.* **20,** 6236–6245.
8. DePace, A. H., Santoso, A., Hillner, P. & Weissman, J. S. (1998) *Cell* **93,** 1241–1252.
9. Liu, J. J. & Lindquist, S. (1999) *Nature* **400,** 573–576.
10. Uptain, S. M. & Lindquist, S. (2002) *Annu. Rev. Microbiol.* **56,** 703–741.
11. Chernoff, Y. O. (2001) *Mutat. Res.* **488,** 39–64.
12. Dobson, C. M. (2001) *Biochem. Soc. Symp.* **68,** 1–26.
13. Scheibel, T., Parthasarathy, R., Sawicki, G., Lin, X. M., Jaeger, H. & Lindquist, S. L. (2003) *Proc. Natl. Acad. Sci. USA*, **100,** 4527–4532.
14. Jarrett, J. T., Berger, E. P. & Lansbury, P. T. (1993) *Biochemistry* **32,** 4693–4697.
15. Lomakin, A., Teplow, D. B., Kirschner, D. A. & Benedek, G. B. (1997) *Proc. Natl. Acad. Sci. USA* **94,** 7942–7947.
16. Blake, C. & Serpell, L. (1996) *Structure (London)* **4,** 989–998.
17. Harper, J. D., Wong, S. S., Lieber, C. M. & Lansbury, P. T. (1997) *Chem. Biol.* **4,** 119–125.
18. Esler, W. P., Stimson, E. R., Jennings, J. M., Vinters, H. V., Ghilardi, J. R., Lee, J. P., Mantyh, P. W. & Maggio, J. E. (2000) *Biochemistry* **39,** 6288–6295.
19. Sparrer, H. E., Santoso, A., Szoka, F. C. & Weissman, J. S. (2000) *Science* **289,** 595–599.
20. Tuite, M. F. (2000) *Science* **289,** 556–557.
21. Wickner, R. B., Taylor, K. L., Edskes, H. K., Maddelein, M. L., Moriyama, H. & Roberts, B. T. (2000) *J. Struct. Biol.* **130**, 310–322.
22. Massi, F. & Straub, J. E. (2001) *Proteins* **42,** 217–229.
23. Tompa, P. (2002) *Trends Biochem. Sci.* **27,** 527–533.
24. Caughey, B. & Lansbury, P. T. (2003) *Annu. Rev. Neurosci.* **26,** 267–298.
25. Thirumalai, D., Klimov, D. K. & Dima, R. I. (2003) *Curr. Opin. Struct. Biol.* **13,** 146–159.
26. Scheibel, T., Kowal, A., Bloom, J. & Lindquist, S. (2001) *Curr. Biol.* **11,** 366–369.
27. Prendergast, F. G., Meyer, M., Carlson, G. L., Iida, S. & Potter, J. D. (1983) *J. Biol. Chem.* **258,** 7541–7544.
28. Shore, J. D., Day, D. E., Francis-Chmura, A. M., Verhamme, I., Kvassman, J., Lawrence, D. A. & Ginsburg, D. (1995) *J. Biol. Chem.* **270,** 5395–5398.
29. Iwatani, S., Iwane, A. H., Higuchi, H., Ishii, Y. & Yanagida, T. (1999) *Biochemistry* **38,** 10318–10323.
30. Hiratsuka, T. (1999) *J. Biol. Chem.* **274,** 29156–29163.
31. Masel, J. & Jansen, V. A. (2000) *Biophys. Chem.* **88,** 47–59.
32. Padrick, S. B. & Miranker, A. D. (2002) *Biochemistry* **41,** 4694–4703.
33. Hammarstrom, P., Wiseman, R. L., Powers, E. T. & Kelly, J. W. (2003) *Science* **299,** 713–716.